Int. J. Multiphase Flow Vol. 14, No. 5, pp. 607–631, 1988
Printed in Great Britain.

0301-9322/88 $3.00 + 0.00

GAS–PARTICLE FLOW IN A DEEP VERTICAL CAVITY DUE TO THERMAL CONVECTION AND PHASE SEPARATION

N. APAZIDIS
Department of Mechanics, Royal Institute of Technology, 100 44 Stockholm, Sweden

(*Received* 31 *July* 1987; *in revised form* 27 *May* 1988)

Abstract—Laminar two-phase flow due to convection and phase separation in a deep vertical cavity with a closed lower end and open upper end, submerged in a homogeneous mixture of gas with solid spherical particles is considered. Analytical expressions for the velocity profiles of each phase, as well as for the total mass and vertical heat fluxes in the two-phase mixture, are obtained and compared with the single-phase case. It is found that the velocity distribution in each phase as well as the direction and the magnitude of the total mass and vertical heat fluxes in the two-phase mixture are essentially controlled by a dimensionless parameter—the ratio of the relative velocity between the phases to the convection velocity in gas.

Key Words: two-phase flow, gas–particle mixture, thermal convection, phase separation, vertical cavity, mass flux, heat flux

1. INTRODUCTION

Natural convection in rectangular cavities has been investigated in numerous publications during the last two decades. Such practical problems as thermal insulation of walls and windows in buildings required an understanding of a heat transfer mechanism between the boundaries. Batchelor (1954) gave a theoretical description of the flow in a vertical cavity. His solution, applied to a fully developed stationary flow, gives a well-known antisymmetric cubic velocity profile with an upward flow in the hot wall region and downward flow in the cold wall region. This investigation was followed by many other, treating the problem of natural convection in vertical slots. For a historical survey see, for example, Chenoweth & Paolucci (1985). The main portion of these investigations is performed within the framework of the Boussinesq approximation, which implies that the ratio of the temperature difference between the walls to their sum is small. An approximation justified for a broad field of applications.

Many areas of modern technology, however, such as chemical engineering, cooling of nuclear reactors, electronics etc., involve flows with large temperature differences. For such flows the Boussinesq approximation is not valid. Chenoweth & Paolucci (1985) investigated gas flows in vertical slots with large temperature differences between the walls, involving temperature-dependent viscosity and conductivity. They presented an analytical solution for the temperature and velocity profiles in the fully developed region of the flow at sufficient distances away from the ends of the cavity.

Broad fields of applications, such as chemical engineering and reactor technology, include processes with flows of mixtures of several components, frequently gas and solid particles. The aim of the present work is to generalize the results of Chenoweth & Paolucci (1985) to a two-phase flow in a deep vertical cavity with a closed lower end and an open upper end, submerged in an infinite region containing a homogeneous mixture of gas with solid spherical particles of equal size. The mixture in the cavity is set into motion as a result of a combined effect of the phase separation, due to the density difference between the phases, and the thermal convection in the gas, due to the temperature difference between the boundaries of the vessel. These two effects are inter-dependent through the interfacial drag force between the components of the mixture. The complexities of the resulting two-phase flow pattern in the neighbourhood of each end of the cavity are beyond the scope of the present work, and the analysis here is restricted to a laminar, fully developed region of the flow, existing at distances sufficiently far from each end of the cavity and on a time scale which is small compared to the time taken to fill the whole vessel with sediment.

Analytical expressions for the temperature and velocity distribution in each phase over the cavity width are obtained both for the case of constant and temperature-dependent conductivity and viscosity and compared to the single-phase case. The mass and vertical heat fluxes in the mixture are then evaluated and the results discussed.

2. FORMULATION

We consider the flow of a mixture in a deep vertical, parallel-plate cavity with a closed lower end and an open upper end. The cavity is submerged in an infinite region containing a homogeneous two-phase mixture of a gas with solid spherical particles of equal size, see figure 1. The mixture flow in the cavity is generated by buoyancy forces due to the temperature difference between the vertical boundaries, and due to the density difference between the phases.

In the present work the mixture of gas and particles is treated as two superimposed continua. Such a description is based on models obtained by taking time averages (Ishii 1975) or volume averages (Nigmatulin 1979), or both (Drew 1971) of the local microscopic balance and constitutive equations for each constituent over regions that are large compared to a typical microstructural dimension of a mixture, e.g. solid particle size. The resulting balance equations for each phase are then formulated in terms of averaged field variables and are valid on our scale, which is large in comparison with dimensions of microstructure. The following investigation is an attempt to apply such a continuum two-phase model (Ishii 1975; Drew & Lahey 1979) to the flow of a gas–particle mixture in a deep laterally heated vertical cavity.

The mixture is therefore treated as two interacting continua, described by means of the corresponding averaged field variables: volume fraction of the dispersed phase α, phase velocities v_k^d and v_k^c, common temperature T, pressure p and the stress tensor of the continuous phase τ_{rk}^c. According to Ishii (1975), the stress tensor of the continuous phase consists of two parts:

$$\tau_{rk}^c = \tau_{rk}^{I} + \tau_{rk}^{II}. \qquad [1]$$

The first part is related to the velocity gradients in the conventional manner for Newtonian fluids,

$$\tau_{rk}^{I} = 2\mu\bar{\bar{d}}_{rk} + 2\lambda\bar{\bar{\bar{d}}}_{rk}, \qquad [2]$$

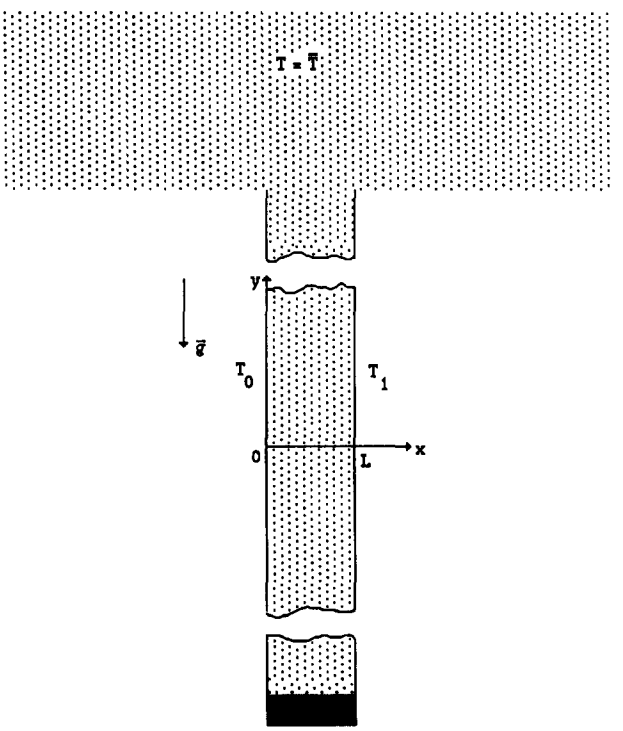

Figure 1. Problem definition.

where $\bar{d}_{rk} = 1/2(v_{r,k} + v_{k,r} - 2/3v_{i,i}\delta_{rk})$ and $\bar{\bar{d}}_{rk} = 1/3v_{i,i}\delta_{rk}$. (Note, that the symbol λ will be subsequently used as the coefficient in the Stokes' drag force.)

The second part of the stress tensor is related to the extra interfacial deformation tensor that arises from the averaging procedure. In the special case when one phase is dispersed, Ishii obtains the following expression:

$$\tau_{rk}^{II} = -\frac{\mu}{2(1-\alpha)}[(v_r^d - v_r^c)(1-\alpha)_{,k} + (v_k^d - v_k^c)(1-\alpha)_{,r}]. \quad [3]$$

The extra interfacial deformation tensor is seen to be zero when α is constant, as will be the case here.

In this specific flow situation where the dispersed phase consists of solid spherical particles of equal size, homogeneously distributed in the continuous carrier phase, the usually proposed form of the stress tensor for the dispersed phase (Ishii 1975; Drew & Lahey 1979; Drew 1983) becomes zero. This in general is an accepted assumption, consistent with neglecting the effects of particle–particle and particle–wall interactions. The details of the two-phase flow in the vicinity of the solid boundaries, where such effects become more significant, are beyond the scope of the present work.

The next item of the employed continuum description of a mixture is the nature of the interaction force between the constituents. This force is often described as a sum of several forces acting on a single particle in a continuous flow field. Besides the Stokes' drag it may include the shear-lift force, due to the uniform shear field of the continuous phase (Saffman 1965), the virtual mass force (Zuber 1964) and the spin-lift force, induced by the inner rotation of a particle (Rubinow & Keller 1961). Each of these forces, acting on a single particle is modified by its own correction factor, which accounts for the finite volume concentration of the dispersed phase. Since here we will assume no inner rotation of the particles and a quasi-steady, one-dimensional flow, the spin-lift and virtual mass forces will be zero. Also the shear-lift force is negligible, compared to the Stokes' drag under the present assumptions, as will be shown at the end of this section.

We neglect therefore the shear-lift force in the first approximation. It should be mentioned at this point, however, that the shear-lift force acts in the direction transverse to the velocity difference between the phases. Incorporation of the shear-lift force in the momentum equations will thus not introduce significant changes in the *vertical* momentum balance. The *horizontal* momentum balance, however, will not be identically satisfied as will be the case here, since the shear-lift force will introduce horizontal particle and gas velocities, which in their turn will influence the particle concentration α. Still, these are according to Di Giovanni & Lee (1974) secondary effects and may be considered as the next step in the analysis of the present problem.

The fluid–solid interaction force per unit volume employed in the present study is thus of the form

$$M_k^d = f(\alpha)F_k \quad [4]$$

and

$$M_k^c = -f(\alpha)F_k, \quad [5]$$

where F_k is the classical Stokes' drag on a single spherical particle,

$$F_k = \lambda\frac{\mu}{a^2}(v_k^c - v_k^d), \quad [6]$$

where $\lambda = 4.5$, μ is the viscosity of the continuous phase and a is the particle radius. The correction factor $f(\alpha)$, accounting for the finite volume fraction of the dispersed phase in the case of spherical particles homogeneously distributed in the continuous phase is of the form

$$f(\alpha) = \frac{4 + 3(8\alpha - 3\alpha^2)^{1/2} + 3\alpha}{(2-3\alpha)^2}\alpha, \quad [7]$$

see Tam (1969).

Further, we assume that the motion of both phases is laminar. This assumption introduces restrictions on the values of the Rayleigh and particle Reynolds numbers. The Rayleigh number

should be less than a certain critical value Ra_c at which the transition towards the multiple-cell motion occurs.

It is well-known that when the value of the Rayleigh number is $< Ra_c$, a fully developed one-dimensional, unicellular flow, parallel to the generators may exist at distances sufficiently far from each end of the cavity. Chenoweth & Paolucci (1985) use the following expression for Ra_c:

$$Ra_c \sim 8 \times 10^3 \, Pr \, (1 - \epsilon^3), \qquad [8]$$

where $Pr = \mu c_p / k$ is the local Prandtl number.

For large temperature differences between the boundaries, [8] gives an upper limit for the distance L between the walls of approx. 0.5 cm. For small temperature differences ($\epsilon \sim 0.1$), $L \sim 1$ cm.

Another assumption, used throughout the paper, is the assumption of the laminar motion of particles. We thus require that the particle Reynolds number $Re_p < 1$,

$$Re_p = \frac{ga^2\gamma}{\lambda v} \frac{a}{v} = \frac{ga^3\gamma}{\lambda v^2} < 1. \qquad [9]$$

This restriction gives an upper limit of the particle radius. For $\gamma = 10^4$, $a < 1.6 \times 10^{-5}$ m, and for $\gamma = 10^3$, $a < 5.5 \times 10^{-4}$ m. The lower limit of the particle radius is approx. 1×10^{-6} m, since for the submicron particles the Brownian motion becomes important.

We now formulate mass, momentum and energy balance equations for the mixture components under the adopted assumptions and approximations. We return again to the specific case of a mixture flow in a deep narrow vertical cavity with closed lower end and open upper end, submerged in an infinite region containing a homogeneous mixture of gas with solid spherical particles of equal size. The vertical y-axis is taken to coincide with the left vertical boundary, which is kept at the absolute temperature T_0. The absolute temperature of the right boundary of the cavity is T_1 ($T_1 > T_0$). The distance between the boundaries in the horizontal direction x is L, as sketched in figure 1. The mixture in the cavity is set into motion as a result of the phase separation, due to the density difference between the phases, and the thermal convection in the gas, due to the temperature difference between the boundaries. These two effects are coupled through the gas–solid interaction force arising from the relative motion of the phases.

Under the present approximations the continuity equation for the dispersed phase

$$\alpha_{,t} + (\alpha v_k^d)_{,k} = 0$$

will in the region sufficiently far from each end of the cavity reduce to

$$\alpha_{,t} = 0. \qquad [10]$$

Momentum equations for each phase in the horizontal direction in the same region, where the flow of the phase is parallel to the generators, reduce to

$$p_{,x} = 0. \qquad [11]$$

According to Kynch (1952), the vertical sedimentation of solid particles may proceed in the three ways, depending on the shape of the curve of the total particle flow rate vs the volume fraction of particles. One of the possible ways is when a direct shock from the initial value of the concentration to the final settled value is formed at the interface of a mixture and sediment settled at the bottom of the vessel. In the remaining two cases a region with a nonuniform concentration of the dispersed phase may be formed between the mixture with the initial concentration of particles at the top and the sediment at the bottom. In the present case of spherical particles in a gas with the initial concentration in the range $0 < \alpha < 0.2$ the first type of sedimentation will occur. Assuming further that the initial concentration of the dispersed phase is constant in the cavity, we obtain by means of [10]

$$\alpha = \text{const.} \qquad [12]$$

We will also consider the process of phase separation on a time scale which is small compared to the time required to fill the whole cavity with sediment. The process is thus regarded as a quasi-steady one and the momentum equations for each phase in the vertical direction are

simplified to

$$0 = -\alpha\rho_d g - \alpha p_y + f(\alpha)\lambda \frac{\mu}{a^2}(v_c - v_d) \quad [13]$$

and

$$0 = -(1-\alpha)\rho_c g - (1-\alpha)p_y + (1-\alpha)(\mu v_{cx})_x - f(\alpha)\lambda \frac{\mu}{a^2}(v_c - v_d). \quad [14]$$

In the case of a quasi-steady, fully developed, homogeneous flow, when the particles and gas are in thermal equilibrium the mixture behaves as a pseudo gas with a modified value of the isentropic exponent, but in all other ways obeys all the well-known relations of thermodynamics, see Wallis (1969). The effect of mutual heat transfer in the horizontal direction is therefore to modify the thermal conductivity k in the energy equation to the value which accounts for the presence of the particles.

The common temperature of gas and particles in the mixture will therefore be distributed in accordance with the energy equation for the pseudo gas,

$$(kT_x)_x = 0, \quad [15]$$

where k is the thermal conductivity of the mixture.

Two more relations are required to close the system of momentum and energy equations.

The first of the closure relations is the equation of state for the gas. Batchelor (1954) argues that, since the pressure differences due to gravity are small compared to the absolute pressure, the variations in the gas density ρ_c are determined entirely by variations in the temperature T,

$$\rho_c T = \text{const.} \quad [16]$$

The second closure relation is a total volume flux condition. In the single-phase case Chenoweth & Paolucci (1985) use the integral condition of zero total mass flow through every cross-section of the enclosed slot to close the system of equations. This condition, however, will not hold in the present case of a sedimentation process in a two-phase mixture, contained in the cavity, due to a combined effect of phase separation and convection. Consider as a simple example the sedimentation of rigid particles in a vertical vessel filled with incompressible liquid and with no temperature difference between the boundaries. At the initial moment the particles are distributed homogeneously and the density of the mixture is therefore constant everywhere in the vessel. As was mentioned earlier, the sedimentation process forms three distinct regions in the vessel, containing dense sediment at the bottom, pure liquid at the top and suspension with constant particle concentration in the middle. Thus a constant density distribution at the initial moment changes to a heavy sediment region at the bottom, a light liquid region at the top and a homogeneous suspension region in the middle. The total volume occupied by these three regions is, however, equal to the volume occupied by the mixture initially. Consider now an arbitrary cross-section of the middle region, occupied by the suspension during the settling process. Sedimentation of particles thus results in a total nonzero mass transport in the downward direction through this section, whereas the total volumetric flow through the same cross-section of the mixture is zero, which is the case of so-called batch sedimentation (Wallis 1969).

In our case the situation is partly similar to the one described above. The difference is that instead of an incompressible liquid we are dealing with a compressible gas and in addition to the effect of gravitational phase separation there is a coupled effect of thermal convection. However, since the pressure differences produced by gravity are small compared to the absolute pressure, the variations in gas density ρ_c will be determined by the variations in the temperature T, which is consistent with the equation of state [16]. Also, here the cavity is considered to be open at the upper end to an infinite region containing a homogeneous mixture with a constant volume fraction of particles, the same as in the cavity. Gas and particles transported in the upward direction will therefore be mixed with the homogeneous suspension in the infinite region. The volume of the mixture and sediment settled on the bottom of the cavity must, however remain unchanged throughout this quasi-stationary process. Also, here we are considering the midregion of the cavity, where the flow is independent of end effects. It will be shown in section 4 that the total mass flux

through every cross-section of the midregion of the cavity is always in the downward direction. The overall flow pattern may therefore be regarded as mass transfer from the infinite two-phase region to the lower end of the cavity, where the dense sediment is settled. An assumption of a zero total volumetric flux through every cross-section of the midregion of the cavity is thus consistent with the approximations introduced earlier.

We therefore close the system of momentum and energy equations by the zero total volume flux condition for the mixture,

$$\int_0^L [\alpha v_d + (1-\alpha)v_c]\,dx = 0. \tag{17}$$

Consider next the set of dimensionless variables

$$\xi = \frac{x}{L}, \tag{18}$$

$$\theta = \frac{T}{\bar{T}}, \tag{19}$$

$$\gamma = \frac{\rho_d}{\bar{\rho}_c}, \tag{20}$$

$$\delta = \frac{a}{L}, \tag{21}$$

$$2\epsilon = \theta_1 - \theta_0, \tag{22}$$

$$k^* = \frac{k}{\bar{k}} \tag{23}$$

and

$$v^* = \frac{v}{\bar{v}}, \tag{24}$$

where $\bar{T}$, $\bar{\rho}_c$, $\bar{k}$ and $\bar{v}$ (kinematic viscosity) are the average quantities (e.g. $\bar{T} = (T_0 + T_1)/2$].

We seek velocity and pressure in the form

$$v_d = \frac{ga^2\gamma}{\lambda\bar{v}} V_d(\xi), \tag{25}$$

$$v_c = \frac{ga^2\gamma}{\lambda\bar{v}} V_c(\xi) \tag{26}$$

and

$$p = -\bar{\rho}_c g y(1 + \gamma P). \tag{27}$$

The zero total volume flux condition, balance of momentum and energy thus take the following nondimensional form:

$$\int_0^1 [\alpha V_d + (1-\alpha)V_c]\,d\xi = 0, \tag{28}$$

$$0 = 1 - \gamma + \gamma P + \gamma \frac{f}{\alpha}\mu^*(V_c - V_d), \tag{29}$$

$$0 = 1 - \frac{1}{\theta} + \gamma P + \frac{\gamma\delta^2}{\lambda}(\mu^* V_{c\xi})_\xi - \gamma\frac{f}{1-\alpha}\mu^*(V_c - V_d) \tag{30}$$

and

$$(k^*\theta_\xi)_\xi = 0, \tag{31}$$

here we have used, according to [16],

$$\frac{\rho_c}{\bar{\rho}_c}=\frac{\bar{T}}{T}=\frac{1}{\theta}. \tag{32}$$

Introducing a new nondimensional variable

$$\Gamma=\frac{\gamma\delta^2}{\lambda} \tag{33}$$

and eliminating V_d by means of [29], a system of equations for V_c, θ and P is obtained:

$$\int_0^1\left(V_c-\frac{\alpha^2}{f}\frac{1-P}{\mu^*}\right)d\xi=0. \tag{34}$$

$$(\mu^* V_{c\xi})_\xi=\frac{1}{\Gamma}\left(\frac{1}{\theta}-1-\gamma\frac{P-\alpha}{1-\alpha}\right) \tag{35}$$

and

$$(k^*\theta_\xi)_\xi=0. \tag{36}$$

The velocity of the dispersed phase is then evaluated by means of [29].

We are assuming here that gas and particles are in thermal equilibrium. The thermal properties of the mixture will be the same as those of a pseudo gas with a modified value of the isentropic exponent. The values of the thermal conductivity and viscosity of the gas must be modified accordingly, to account for the presence of the particles. However, since we assume a homogeneous particle distribution in the cavity, the ratio of the local value of k to the average value $\bar{k}$ for the mixture is the same as for the pure gas. The same applies to the viscosity. We are therefore able to use the same relations for the nondimensional conductivity $k^*=k/\bar{k}$ and viscosity $\mu^*=\mu/\bar{\mu}$ as for the pure gas. Variation of the nondimensional conductivity and viscosity with temperature may therefore be obtained by means of Sutherland's laws for gases (White 1974):

$$k^*=\frac{(1+S_k)\theta^{3/2}}{\theta+S_k} \tag{37}$$

and

$$\mu^*=\frac{(1+S_\mu)\theta^{3/2}}{\theta+S_\mu}. \tag{38}$$

Values of the constants S_k and S_μ will be given in section 3.

We now return for a moment to the beginning of this section and show by means of the dimensionless parameters introduced earlier, that the shear-lift force in the present flow situation is negligible compared to the Stokes' drag. According to Saffman (1965),

$$L_s=6.46\,\mu a^2\left|\frac{S}{\nu}\right|^{1/2}(v_c-v_d), \tag{39}$$

where S is the velocity gradient of the fluid. The ratio of the shear-lift force to the Stokes' drag force is thus

$$\left|\frac{L_s}{F_s}\right|=\frac{6.46\,\mu a^2\left|\frac{S}{\nu}\right|^{1/2}|v_c-v_d|}{6\pi\mu a|v_c-v_d|}\sim\left(\frac{|S|a^2}{\nu}\right)^{1/2}\sim\left(\frac{ga^2\gamma}{\lambda\nu}\frac{a}{\nu}\frac{a}{L}\right)^{1/2}=(\mathrm{Re}_p\delta)^{1/2}\ll 1. \tag{40}$$

3. VELOCITY PROFILES

Similarly to Chenoweth & Paolucci (1985), we consider first the solution in the case of constant conductivity and viscosity, $k^*=\mu^*=1$. The constant property case may be applied to flows with small temperature differences between the boundaries. As the temperature difference increases the constant property assumption becomes less realistic and variations of the viscosity and conductivity

must be taken into account. The constant property case will, therefore, mainly serve as a reference solution for the greater temperature differences. Comparing this solution with the case of a temperature-dependent k^* and μ^* we will be able to highlight the influence of the conductivity and viscosity variations on various two-phase flow parameters.

Solution of the energy equation [36] gives in this case a well-known linear distribution of the temperature between the vertical boundaries:

$$\theta = 1 + \epsilon(2\xi - 1), \qquad [41]$$

see Batchelor (1954).

Introducing [41] into [35] and solving [34] and [35] we obtain the velocity profile of the continuous phase V_c and the pressure term P. The velocity of the dispersed phase is then evaluated by means of [29], see appendix A. The corresponding curves are displayed in figures 2–4.

In the single-phase case, investigated in detail by Chenoweth & Paolucci (1985), the flow is regulated by means of thermal convection, due to the temperature difference between the boundaries. This is also an important effect in the case of two-phase flow. In the present work, however, there is an additional coupled effect of the gravitational separation of the phases. These two effects influence one another through the fluid–solid interaction force. The relative significance of these two features of the flow is given by the value of the dimensionless parameter Γ, introduced in [33]. Consider the ratio of the particle velocity in the stagnant fluid to the convection velocity in the gas,

$$\frac{v_{\text{part}}}{v_{\text{conv}}} \sim \frac{\dfrac{ga^2\gamma}{\lambda\nu}}{\text{Ra}\,\dfrac{\kappa}{L}} = \frac{ga^2\gamma}{\lambda\nu}\,\frac{\nu}{gL^2 2\epsilon} = \frac{\gamma\delta^2}{\lambda 2\epsilon} \sim \Gamma, \qquad [42]$$

where Ra is the Rayleigh number and κ is the thermal diffusivity, Γ is thus of the same order of magnitude as the ratio of the particle velocity in the stagnant fluid to the convection velocity, when ϵ is in the range $0.1 \leqslant \epsilon \leqslant 1$. Next we list a number of values of $\Gamma = \gamma\delta^2/\lambda$ and the corresponding values of γ and δ ($\lambda = 4.5$) that will be used subsequently throughout this paper:

(1) $\Gamma = 2 \times 10^{-4}$, $\gamma = 10^3$, $\delta = 10^{-3}$;

(2) $\Gamma = 2 \times 10^{-3}$, $\gamma = 10^4$, $\delta = 10^{-3}$;

(3) $\Gamma = 10^{-2}$, $\gamma = 5 \times 10^3$, $\delta = 10^{-2}$;

(4) $\Gamma = 2 \times 10^{-2}$, $\gamma = 10^3$, $\delta = 10^{-2}$;

(5) $\Gamma = 0.2$, $\gamma = 10^4$, $\delta = 10^{-2}$;

(6) $\Gamma = 2$, $\gamma = 10^4$, $\delta = 0.03333$.

Small values of Γ, e.g. $\Gamma = 2 \times 10^{-4}$, 2×10^{-3} and $\Gamma = 2 \times 10^{-2}$, as in figure 2, indicate that the separation velocity of the phases is small compared to the convection velocity. The effect of thermal convection is thus dominating at small values of Γ and the velocity profiles of the continuous phase reveal certain similarities to those of a single-phase case [see Chenoweth & Paolucci (1985) for large ϵ-values] and reduce to the cubic velocity profile of Batchelor (1954) for small ϵ-values. An important distinction between the present case and the one considered by Chenoweth & Paolucci is the assumption of zero total volumetric flux of the two-phase mixture, discussed in section 2, in contrast to the assumption of zero mass flux for the closed slots used by Chenoweth & Paolucci. As a direct result of this, the zero velocity points remain relatively fixed in ξ as ϵ increases, see figure 2(a), while those of Chenoweth & Paolucci translate nearly linearly with ϵ toward the cold wall. These two different assumptions reduce, however, to a common form used for an incompressible fluid in the Boussinesq approximation valid at small temperature differences between the boundaries. The velocity profiles in the present work and those of Chenoweth & Paolucci reduce, therefore, to the antisymmetric cubic velocity distribution of Batchelor (1954).

For small Γ-values the relative velocity between the phases is small, giving velocity profiles of the dispersed phase that are close to those of the continuous phase. Furthermore, assumption of

constant viscosity results in a constant relative velocity between the phases over the cavity width. This means that the velocity profiles of the dispersed phase for various ϵ-values are simply obtained by shifting the corresponding profiles by a value equal to the relative velocity beween the phases.This property will certainly not hold in the case of temperature-dependent viscosity. As will

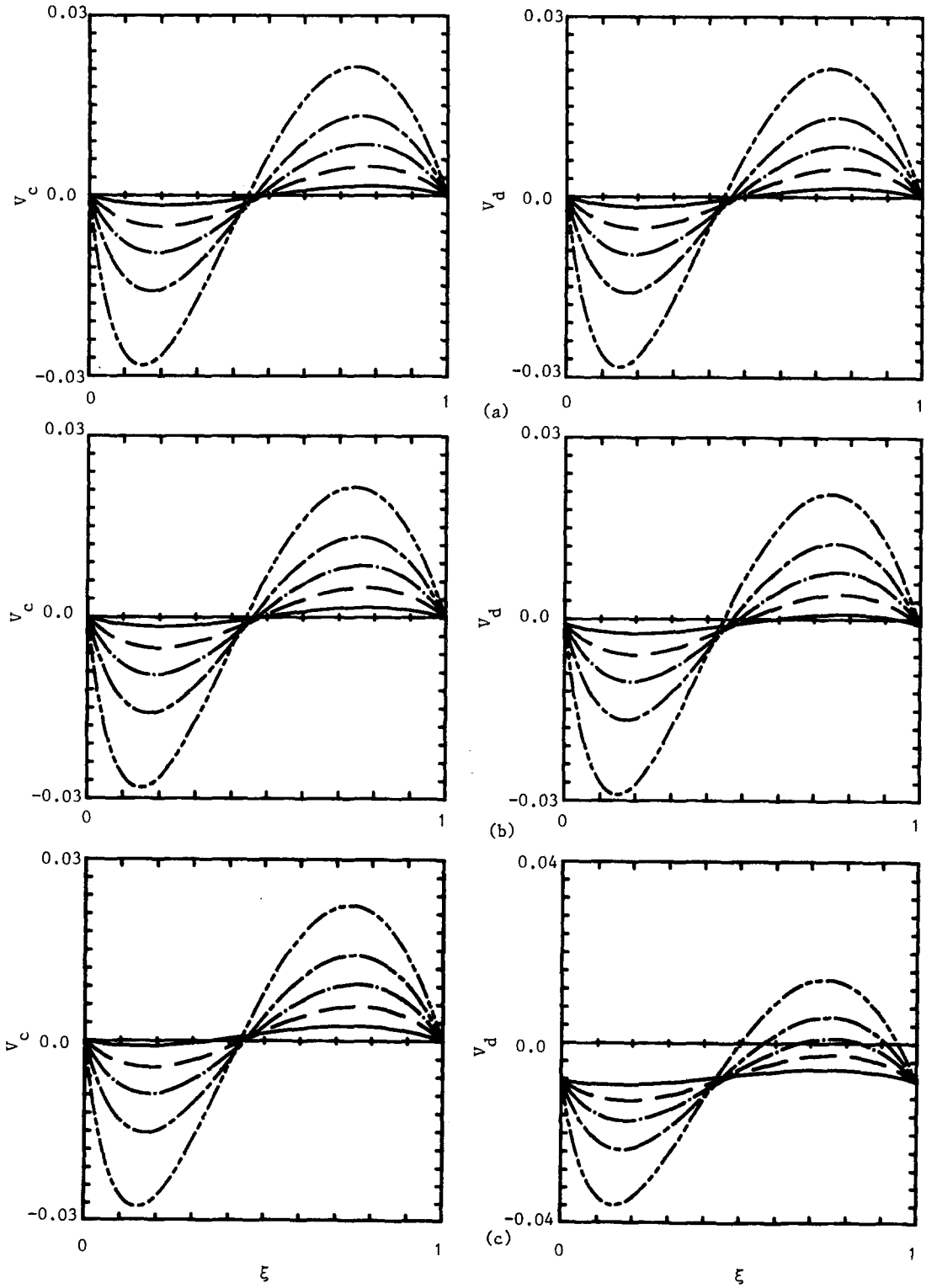

Figure 2. Velocity profiles of the phases for temperature-independent k^* and μ^*. —— $\epsilon = 0.1$, – – – $\epsilon = 0.3$, —·— $\epsilon = 0.5$, ———— $\epsilon = 0.7$, ———— $\epsilon = 0.9$; $\alpha = 0.1$. (a) $\Gamma = 2 \times 10^{-4}$, (b) $\Gamma = 2 \times 10^{-3}$, (c) $\Gamma = 2 \times 10^{-2}$.

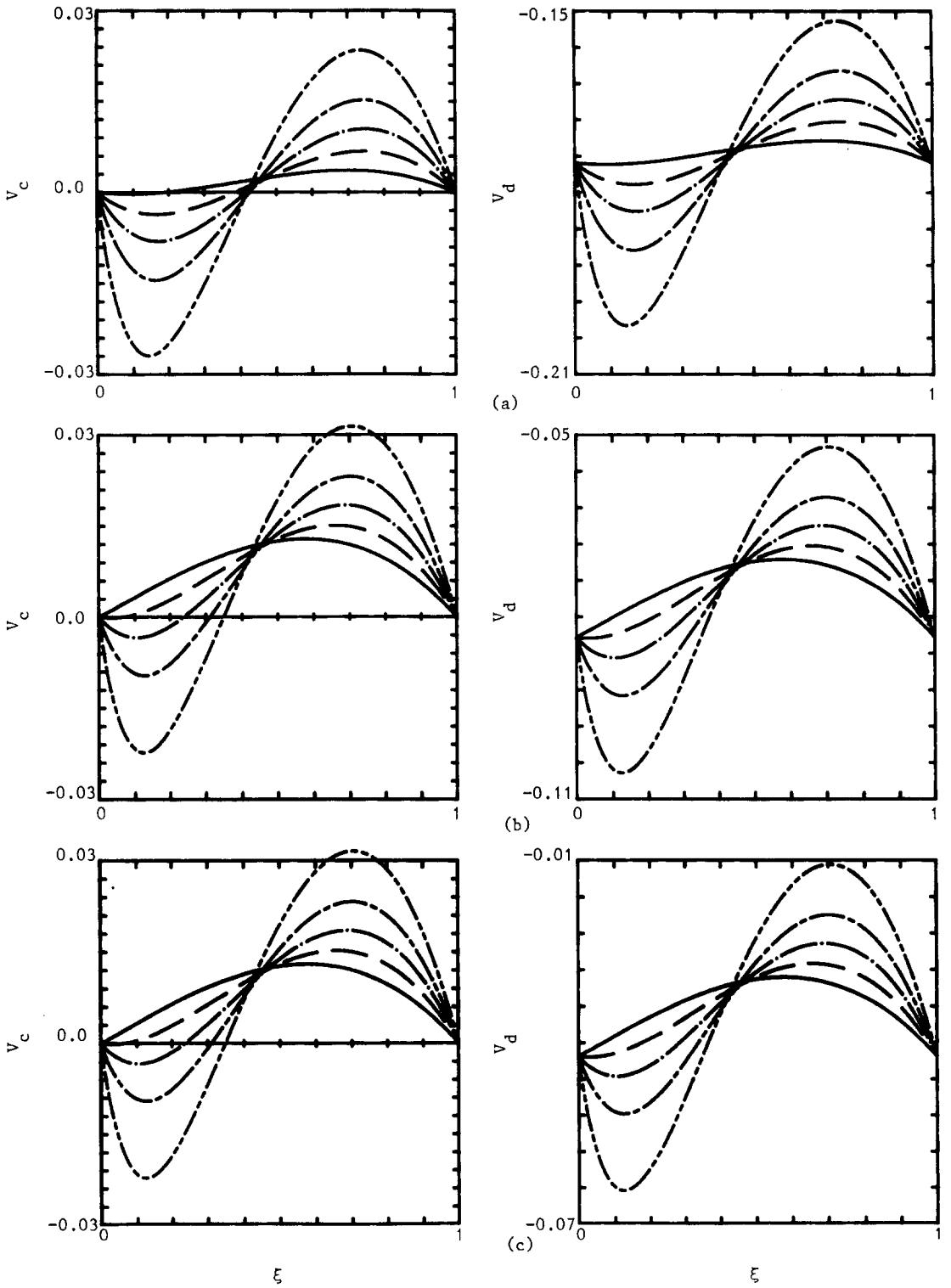

Figure 3. Velocity profiles of the phases for temperature-independent k^* and μ^*. —— $\epsilon = 0.1$, – – – $\epsilon = 0.3$, —·— $\epsilon = 0.5$, —— —— $\epsilon = 0.7$, ———— $\epsilon = 0.9$; $\Gamma = 0.2$. (a) $\alpha = 0.01$, (b) $\alpha = 0.1$, (c) $\alpha = 0.2$.

be shown later, the relative velocity and, thus, the mutual interaction force between the phases are strongly dependent upon variable viscosity.

For intermediate values of Γ, e.g. $\Gamma = 0.2$, as in figure 3, both the effects of phase separation and thermal convection are important. The velocity profiles of the continuous phase still resemble the single-phase case. Here, however, the curves are more asymmetric, indicating that the gas flows

in the upward direction over the entire cavity width for small temperature differences ϵ, contrary to the single-phase case. The relative velocity between the phases becomes significant in this case and the particles flow in the downward direction, as shown in figure 3. By increasing the volume concentration of particles α from 0.01, as in figure 3(a), to 0.2, as in figure 3(c), we increase the interaction force beween the phases and reduce the relative velocity.

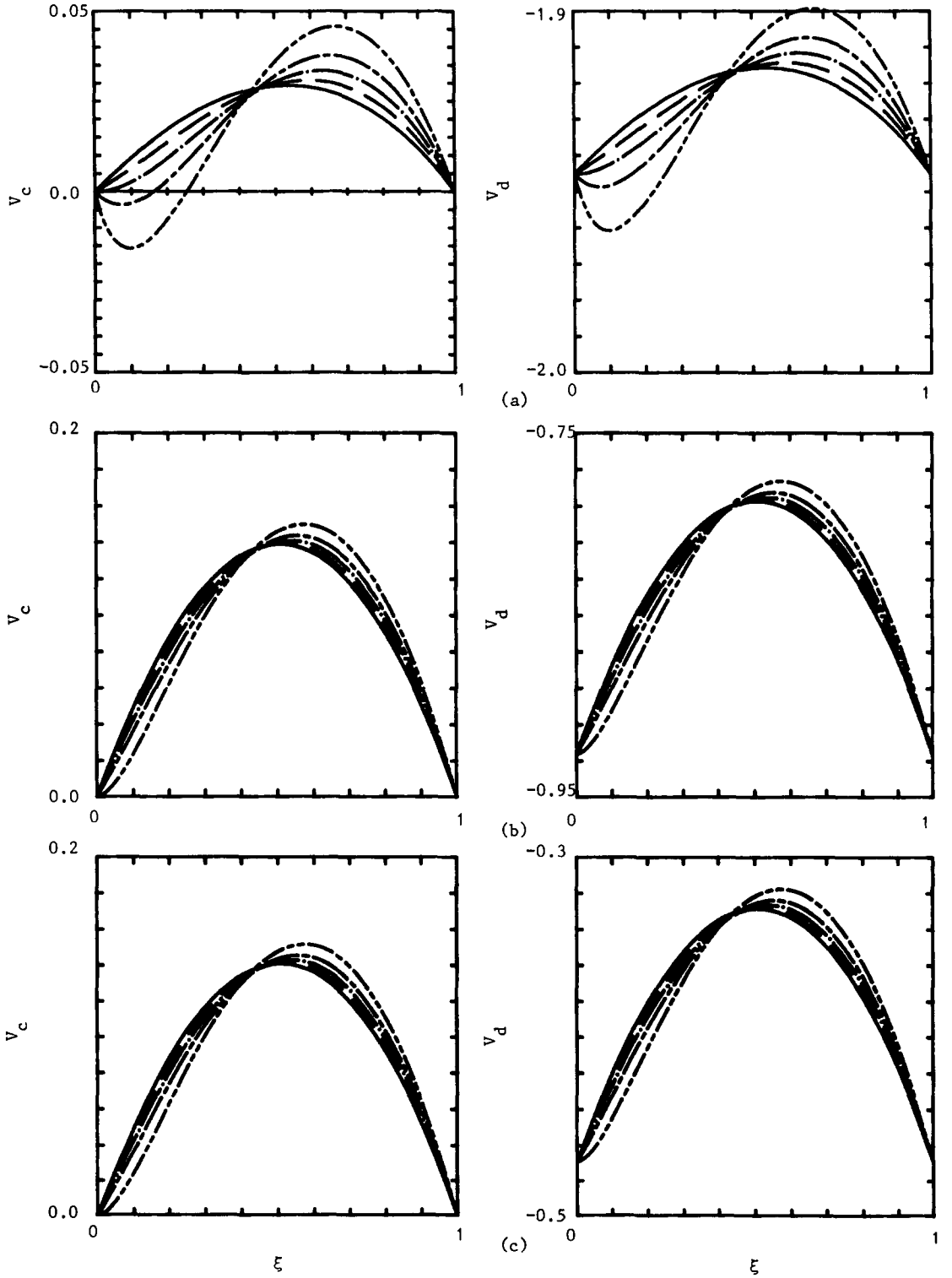

Figure 4. Velocity profiles of the phases for temperature-independent k^* and μ^*. —— $\epsilon = 0.1$, — — $\epsilon = 0.3$, —·— $\epsilon = 0.5$, ——— $\epsilon = 0.7$, ———— $\epsilon = 0.9$, $\Gamma = 2$. (a) $\alpha = 0.01$, (b) $\alpha = 0.1$, (c) $\alpha = 0.2$.

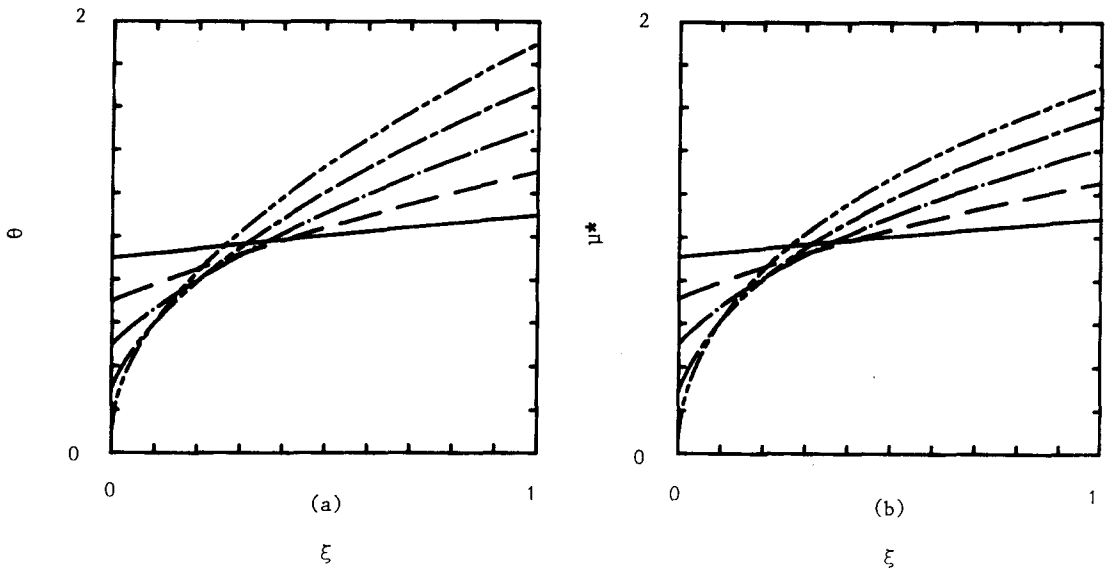

Figure 5. Temperature and viscosity distributions in the slot. —— $\epsilon = 0.1$, —— $\epsilon = 0.3$, —·— $\epsilon = 0.5$, ——— $\epsilon = 0.7$, ——— $\epsilon = 0.9$.

For larger values of Γ the effect of the gravitational separation of the phases becomes dominating. For $\Gamma = 2$, as in figure 4, the flow of the phases is mainly controlled by the gravitational separation of the phases with an upward flow of gas and downward flow of particles. The curves for various ϵ-values converge and the relative velocity between the phases increases. An increase in the volume concentration α further amplifies the effect of gravitational separation on the flow pattern.

Next, we choose as a starting point for our calculations a more realistic, for the greater ϵ-values, assumption of temperature-dependent conductivity and viscosity varying in accordance with Sutherland's law [37] and [38]. For the purpose of comparison with the single-phase case we will use the same example as Chenoweth & Paolucci (1985), namely air with $T = 300$ K, $S_k = 0.648$ and $S_\mu = 0.368$. These values may be found in White (1974).

The temperature distribution is no longer linear and is obtained by means of the energy equation [36] along with [37]. As suggested by Chenoweth & Paolucci (1985), we will use temperature θ as an independent variable. The expression for the transverse coordinate ξ as function of θ is given in appendix B and is the same as in the single-phase case. Further, using

$$\frac{dV_c}{d\xi} = \frac{dV_c}{d\theta}\frac{d\theta}{d\xi}, \qquad [43]$$

[34]–[38] and [29], we obtain expressions for $V_d(\theta)$, $V_c(\theta)$ and P, see appendix B.

Variations of the dimensionless temperature and viscosity across the slot width are shown in figure 5 and are the same as in the single-phase case. Velocity profiles of the phases for various Γ-values are displayed in figures 6–8.

For $\Gamma = 2 \times 10^{-4}$ the effect of thermal convection is dominating, the relative velocity between the phases is less significant and the velocity profiles of the continuous phase are similar in part to those of a single-phase case, see Chenoweth & Paolucci (1985). The zero velocity points show here a greater shift toward the cold wall with growing ϵ-values than in the constant property case, see figure 6(a). This shift is nevertheless smaller than that of the single-phase case, as a result of the different assumptions, as discussed in section 2. Due to small values of the relative velocity, profiles of the dispersed phase are close to those of the continuous phase. As compared to the case of constant conductivity and viscosity, the spacing between the curves corresponding to different ϵ-values here becomes independent of ϵ, which is also true in the case of single-phase flow. In figure 6(c), $\Gamma = 2 \times 10^{-2}$. The effect of the gravitational separation becomes somewhat greater than in the previous figures. The motion is still mainly controlled by thermal convection. Influence of the variable viscosity on the velocity of the dispersed phase becomes noticeable, especially for the

higher values of ϵ. The relative velocity increases rapidly near the cold wall. This abrupt increase in the relative velocity in the vicinity of the cold wall is due to the rapid decrease of the dimensionless viscosity, which approaches zero with an infinite gradient as ϵ approaches unity, see figure 5(b).

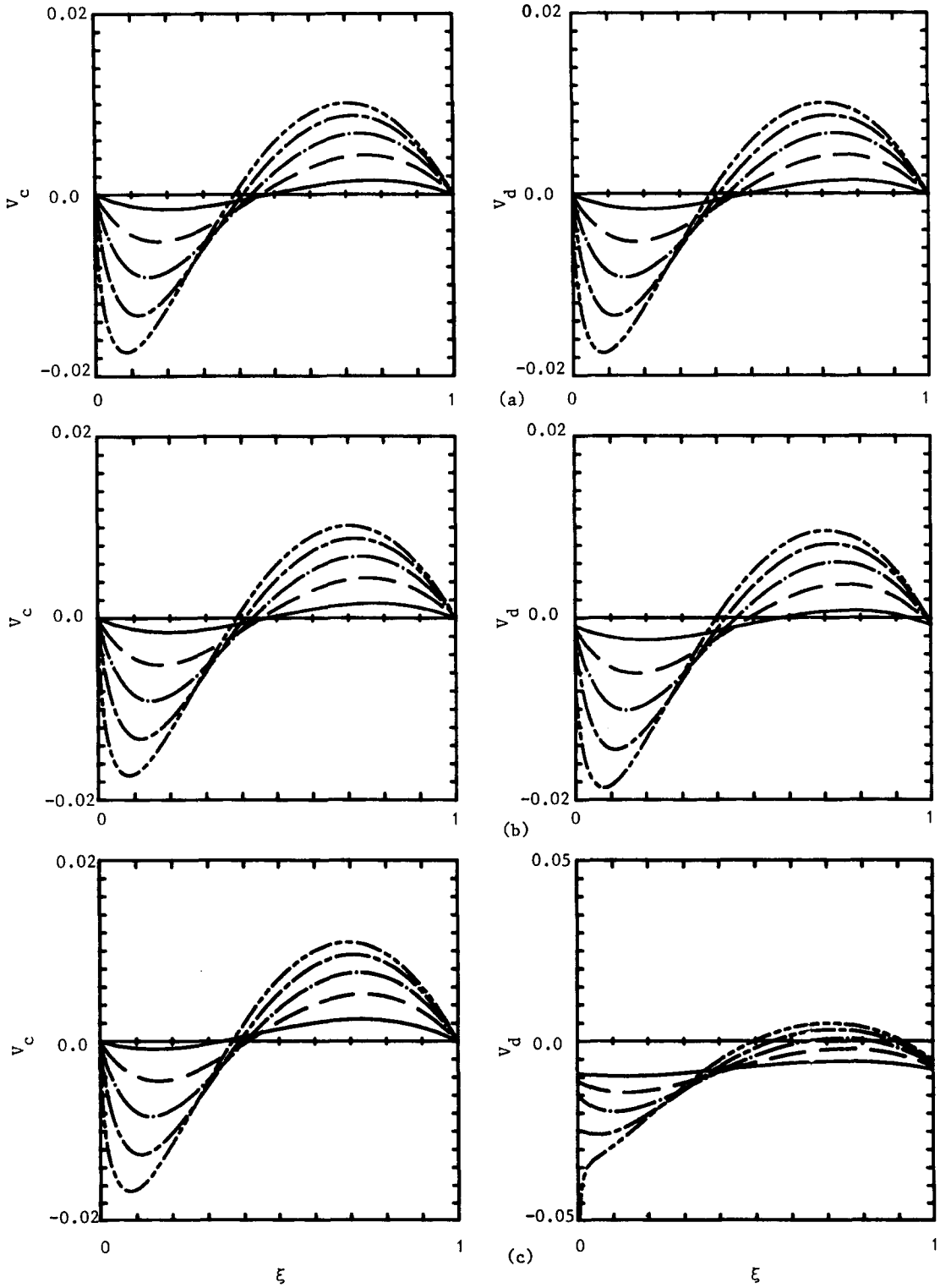

Figure 6. Velocity profiles of the phases for temperature-dependent k^* and μ^*. —— $\epsilon = 0.1$, —— $\epsilon = 0.3$, —·— $\epsilon = 0.5$, ——— $\epsilon = 0.7$, ———— $\epsilon = 0.9$; $\alpha = 0.1$. (a) $\Gamma = 2 \times 10^{-4}$, (b) $\Gamma = 2 \times 10^{-3}$, (c) $\Gamma = 2 \times 10^{-2}$.

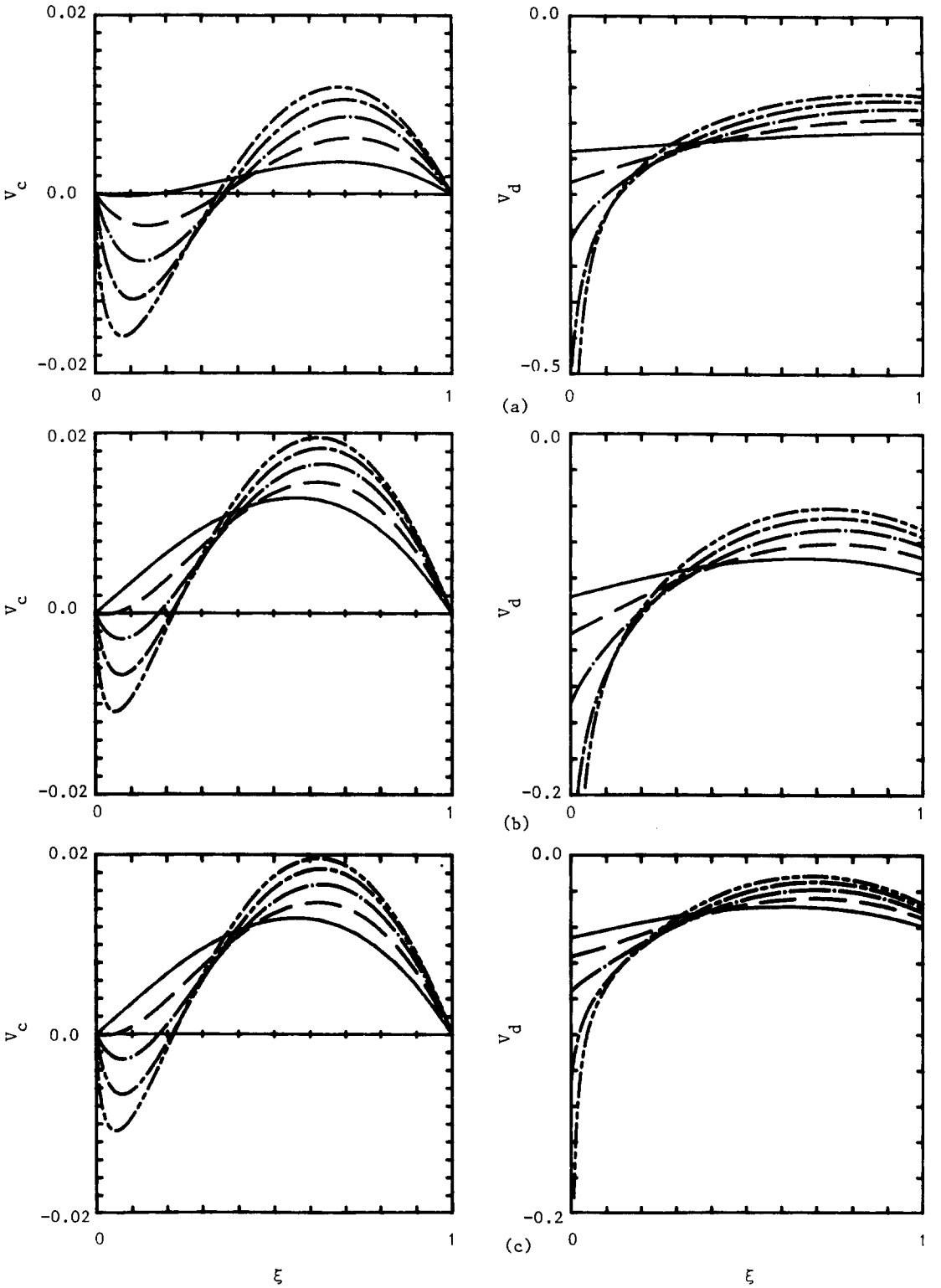

Figure 7. Velocity profiles of the phases for temperature-dependent k^* and μ^*. —— $\epsilon = 0.1$, —— $\epsilon = 0.3$, —·— $\epsilon = 0.5$, —— $\epsilon = 0.7$, ——— $\epsilon = 0.9$; $\Gamma = 0.2$. (a) $\alpha = 0.01$, (b) $\alpha = 0.1$, (c) $\alpha = 0.2$.

For intermediate values of Γ, e.g. $\Gamma = 0.2$, as in figure 7, both thermal convection and the gravitational separation are equally important. Velocity profiles of the continuous phase here are more asymmetric than in the case of constant conductivity and viscosity. Here we obtain a unidirectional upward gas flow over almost the entire cavity width for $\alpha = 0.1$ and $\alpha = 0.2$. A

downward flow of gas exists only in the narrow region in the vicinity of the cold wall for $\epsilon > 0.4$. The dispersed phase flows in the downward direction throughout the whole cavity. Because of the viscosity variation over the cavity, the velocity profiles of the dispersed phase are no longer obtained by a simple shift of the corresponding velocity profiles of the continuous phase in the

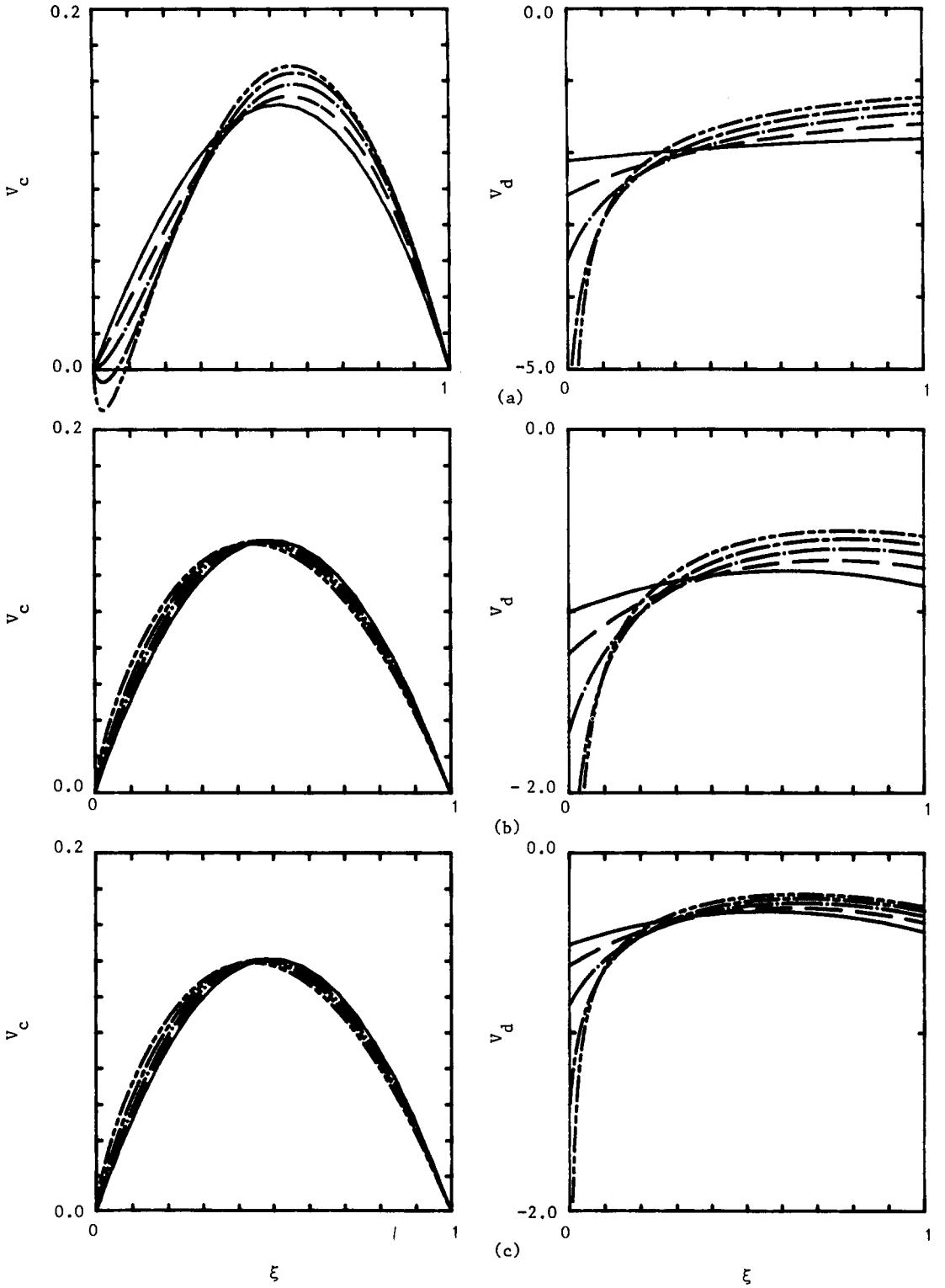

Figure 8. Velocity profiles of the phases for temperature-dependent k^* and μ^*. —— $\epsilon = 0.1$, —— $\epsilon = 0.3$, —·— $\epsilon = 0.5$, —— $\epsilon = 0.7$, ——— $\epsilon = 0.9$, $\Gamma = 2$. (a) $\alpha = 0.01$, (b) $\alpha = 0.1$, (c) $\alpha = 0.2$.

vertical direction. The relative velocity between the phases increases near the cold wall and decreases near the hot wall as the temperature difference between the boundaries grows. Growth of the relative velocity near the cold wall is, however, far more rapid than its decrease at the hot wall. This leads to an increasing asymmetry in the velocity profiles of the dispersed phase as ϵ approaches unity, see figure 7.

If the value of Γ is increased, e.g. to 2, as in figure 8, the character of the two-phase flow becomes dominated by the gravitational separation of the phases. This means that the continuous phase flows in the upward direction and the particles are raining down. The velocity profiles of the continuous phase become more and more ϵ-independent and symmetric with a maximum shifting towards the middle position between the boundaries. Velocity profiles of the dispersed phase are, however, still asymmetric, mainly due to an abrupt increase in the relative velocity at the cold wall, with a growing temperature difference between the walls, see figure 8.

4. MASS AND HEAT FLUXES

Using the obtained velocity distributions it is now possible to evaluate mass and heat fluxes for each phase, as well as the total vertical mass and heat transfer in the mixture.

We define the following dimensionless mass fluxes per unit volume of the flow field:

$$\mathrm{d}g_\mathrm{d} = \alpha\rho_\mathrm{d}v_\mathrm{d} = \frac{ga^2\gamma}{\lambda\bar{\nu}}\bar{\rho}_\mathrm{c}\,\mathrm{d}G_\mathrm{d} \qquad [44]$$

and

$$\mathrm{d}g_\mathrm{c} = (1-\alpha)\rho_\mathrm{c}v_\mathrm{c} = \frac{ga^2\gamma}{\lambda\bar{\nu}}\bar{\rho}_\mathrm{c}\,\mathrm{d}G_\mathrm{c}. \qquad [45]$$

Integration over the cavity width gives

$$G_\mathrm{d} = \gamma\alpha\int_0^1 V_\mathrm{d}\,\mathrm{d}\xi \qquad [46]$$

and

$$G_\mathrm{c} = \gamma(1-\alpha)\int_0^1 \frac{\rho_\mathrm{c}}{\bar{\rho}_\mathrm{c}}V_\mathrm{d}\,\mathrm{d}\xi. \qquad [47]$$

Since θ serves as an independent variable in the case of temperature-dependent properties, [46] and [47] are transformed into

$$G_\mathrm{d} = \frac{\gamma\alpha}{\mathrm{c}_1}\int_{\theta_0}^{\theta_1} V_\mathrm{d}(1+\mathrm{S}_k)\theta^{3/2}(\mathrm{S}_k+\theta)^{-1}\,\mathrm{d}\theta \qquad [48]$$

and

$$G_\mathrm{c} = \frac{(1-\alpha)}{\mathrm{c}_1}\int_{\theta_0}^{\theta_1} V_\mathrm{c}(1+\mathrm{S}_k)\theta^{1/2}(\mathrm{S}_k+\theta)^{-1}\,\mathrm{d}\theta, \qquad [49]$$

by means of

$$\mathrm{d}\xi = \frac{k}{\mathrm{c}_1}\mathrm{d}\theta = \frac{(1+\mathrm{S}_k)\theta^{3/2}(\theta+\mathrm{S}_k)^{-1}}{\mathrm{c}_1}\mathrm{d}\theta. \qquad [50]$$

The total heat flux per unit volume of the two-phase flow is

$$\mathrm{d}q = \mathrm{d}q_\mathrm{d} + \mathrm{d}q_\mathrm{c} = \alpha\rho_\mathrm{c}v_\mathrm{d}T + (1-\alpha)\rho_\mathrm{c}v_\mathrm{c}T, \qquad [51]$$

since $T_y = 0$. The total dimensionless heat flux in the mixture is therefore of the form

$$q = \frac{ga^2\gamma}{\lambda\bar{\nu}}\bar{\rho}_\mathrm{c}\bar{T}(Q_\mathrm{d}+Q_\mathrm{c}) = \frac{ga^2\gamma}{\lambda\bar{\nu}}\bar{\rho}_\mathrm{c}\bar{T}\left[\frac{\gamma\alpha}{\mathrm{c}_1}\int_{\theta_0}^{\theta_1} V_\mathrm{d}\theta(1+\mathrm{S}_k)\theta^{3/2}(\mathrm{S}_k+\theta)^{-1}\mathrm{d}\theta + \frac{(1-\alpha)}{\mathrm{c}_1}\int_{\theta_0}^{\theta_1} V_\mathrm{c}(1+\mathrm{S}_k)\theta^{3/2}(\theta+\mathrm{S}_k)^{-1}\mathrm{d}\theta\right]. \qquad [52]$$

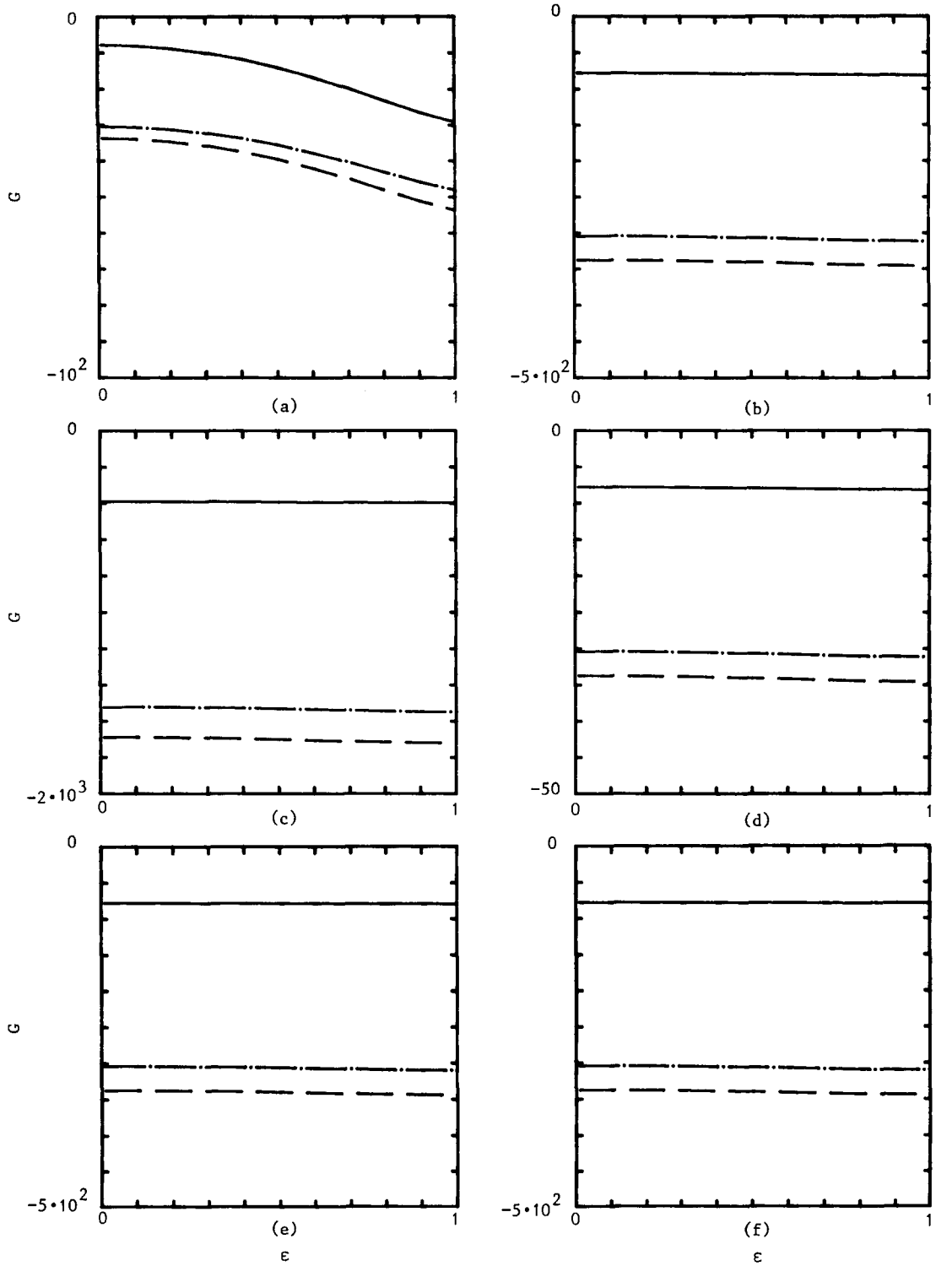

Figure 9. Total mass flux vs scaled temperature difference between the boundaries. —— $\alpha = 0.01$, – – – $\alpha = 0.1$, —·— $\alpha = 0.2$. (a) $\Gamma = 2 \times 10^{-4}$, (b) $\Gamma = 2 \times 10^{-3}$, (c) $\Gamma = 10^{-2}$, (d) $\Gamma = 2 \times 10^{-2}$, (e) $\Gamma = 0.2$, (f) $\Gamma = 2$.

Mass and vertical heat fluxes are shown for various Γ-values as functions of the scaled temperature difference ϵ and the volume fraction of the dispersed phase α.

As already discussed, we use an assumption of the zero total volume flux in the present flow situation instead of the zero mass flux assumption for the case of single-phase flow in a closed slot used by Chenoweth & Paolucci (1985).

Figure 9 shows that the total mass flux is always negative (in the downward direction) and becomes insensitive to the temperature difference ϵ for $\Gamma \geqslant 2 \times 10^{-3}$. Figure 10 suggests, on the other hand, that the magnitude of the mass flux is not simply increased by an increase in the volume fraction of the dispersed phase α, but that it reaches a maximum at a value of $\alpha = 0.12$. This is due to the fact that by increasing the volume fraction α we increase the interaction force between

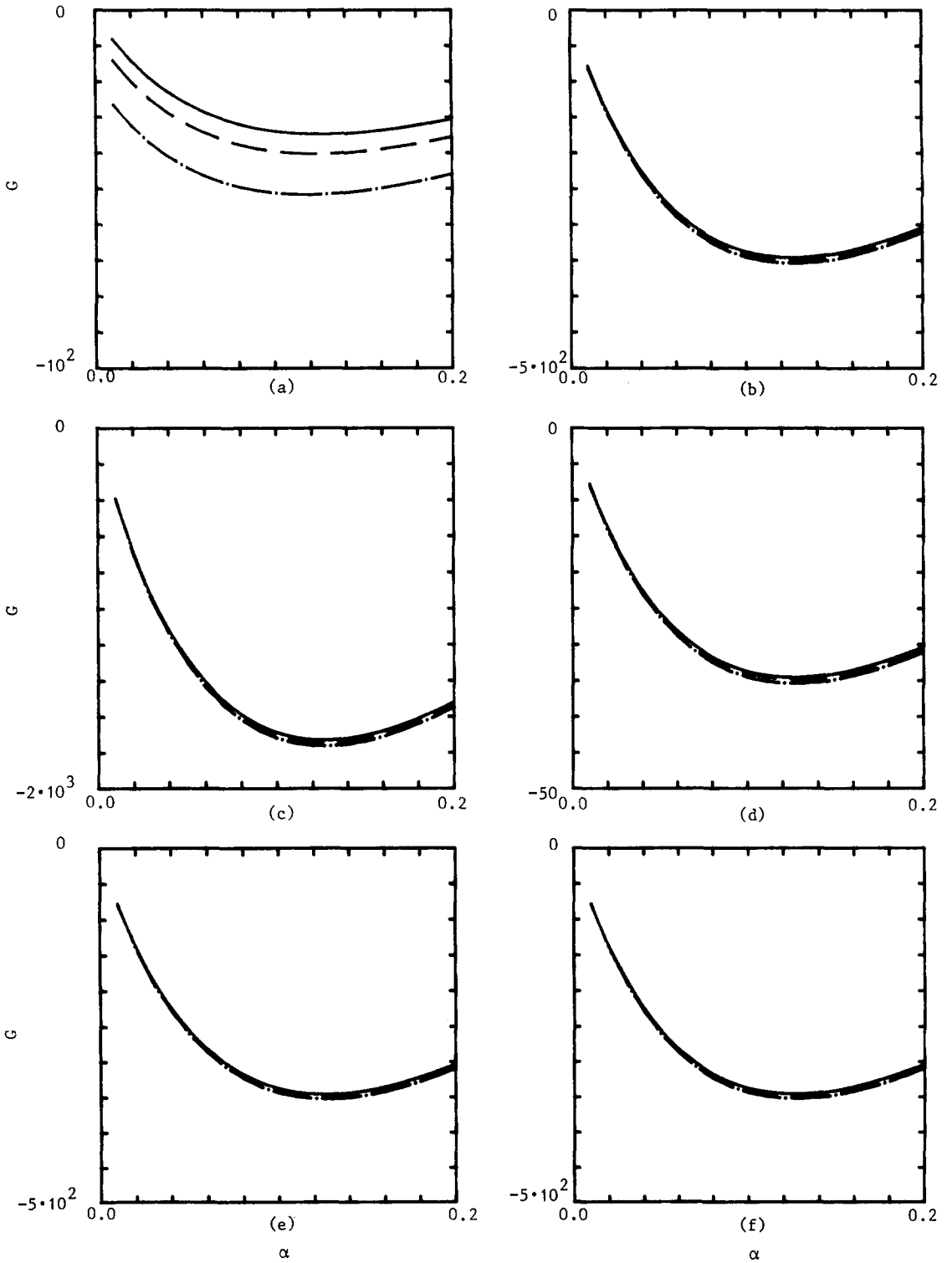

Figure 10. Total mass flux vs volume fraction of particles. —— $\epsilon = 0.1$, —— $\epsilon = 0.5$, —·— $\epsilon = 0.9$. (a) $\Gamma = 2 \times 10^{-4}$, (b) $\Gamma = 2 \times 10^{-3}$, (c) $\Gamma = 10^{-2}$, (d) $\Gamma = 2 \times 10^{-2}$, (e) $\Gamma = 0.2$, (f) $\Gamma = 2$.

the phases, which leads to a decrease in the relative velocity. Although the mass of the dispersed phase, which accounts for the dominating portion of the mass of the two-phase flow, is increased, the magnitude of the mass flux may be decreased as a result of retardation of the particle flow.

Figures 11 and 12 display the mass flux of the gas as function of ϵ and α for various Γ-values. It is seen that the direction of the flux is controlled by the value of Γ. The mass flux of the gas

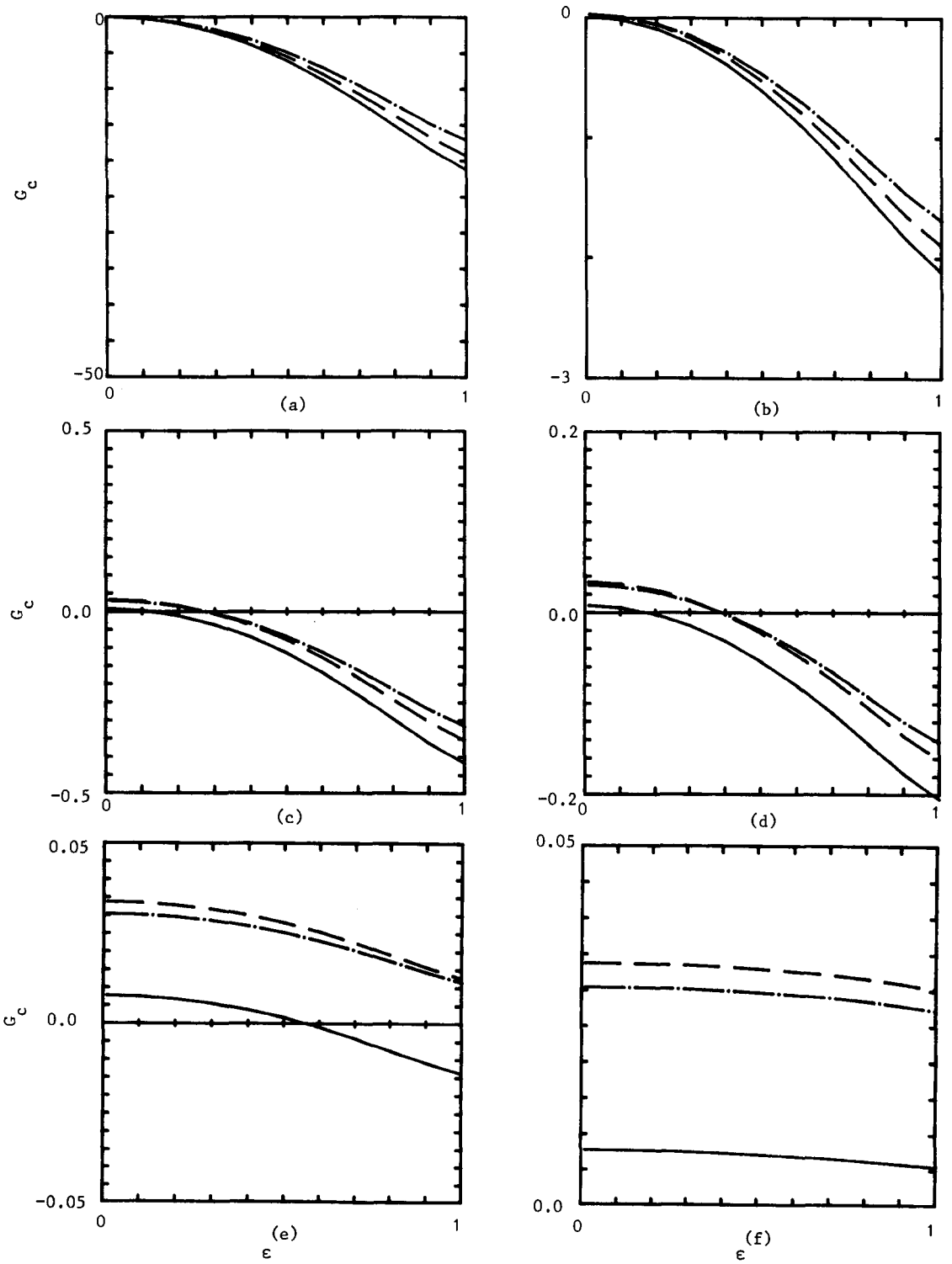

Figure 11. Gas mass flux vs scaled temperature difference between the boundaries. —— $\alpha = 0.01$, –– $\alpha = 0.1$, —·— $\alpha = 0.2$. (a) $\Gamma = 2 \times 10^{-4}$, (b) $\Gamma = 2 \times 10^{-3}$, (c) $\Gamma = 10^{-2}$, (d) $\Gamma = 2 \times 10^{-2}$, (e) $\Gamma = 0.2$, (f) $\Gamma = 2$.

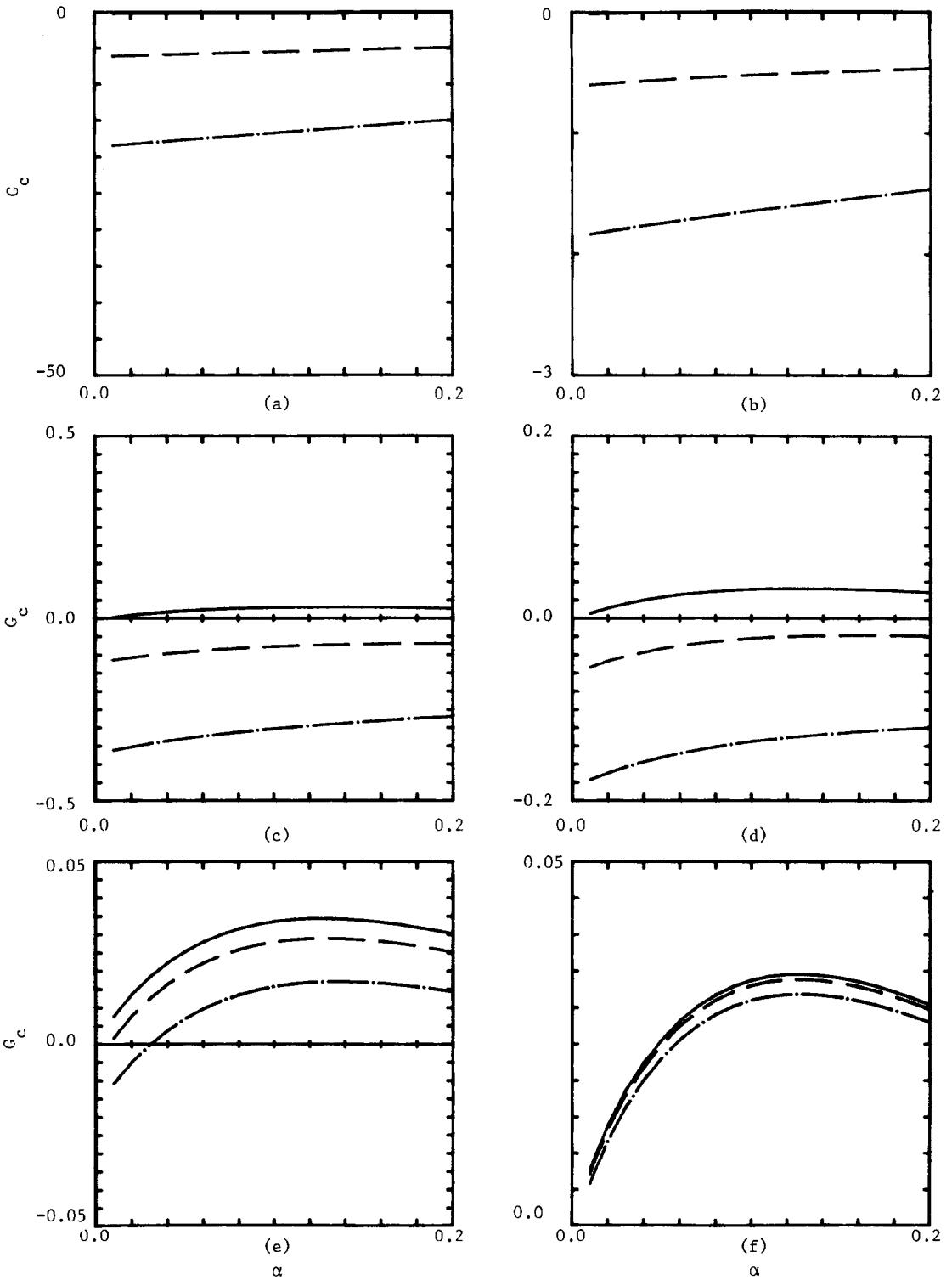

Figure 12. Gas mass flux vs volume fraction of particles. —— $\epsilon = 0.1$, — — $\epsilon = 0.5$, —·— $\epsilon = 0.9$.
(a) $\Gamma = 2 \times 10^{-4}$, (b) $\Gamma = 2 \times 10^{-3}$, (c) $\Gamma = 10^{-2}$, (d) $\Gamma = 2 \times 10^{-2}$, (e) $\Gamma = 0.2$, (f) $\Gamma = 2$.

is entirely negative for the small values of Γ, in either direction for the intermediate values, and becomes positive for $\Gamma = 2$. It decreases with growing ϵ, increases with α or has a maximum at $\alpha = 0.12$ for large values of Γ. At large values of Γ the flow becomes dominated by the gravitational separation of the phases with particles raining down and gas flowing in the upward direction with a nearly parabolic velocity distribution which results in a positive mass flux of the gas.

It is noteworthy that although the total volume flux of the two-phase flow is always zero, the mass fluxes of each phase need not be and are not always in different directions. The mass flux of the gas is in the same downward direction as the mass flux of the particles for small values of Γ and for intermediate values at greater temperature differences, see figures 11(a–d) and 12(a–d).

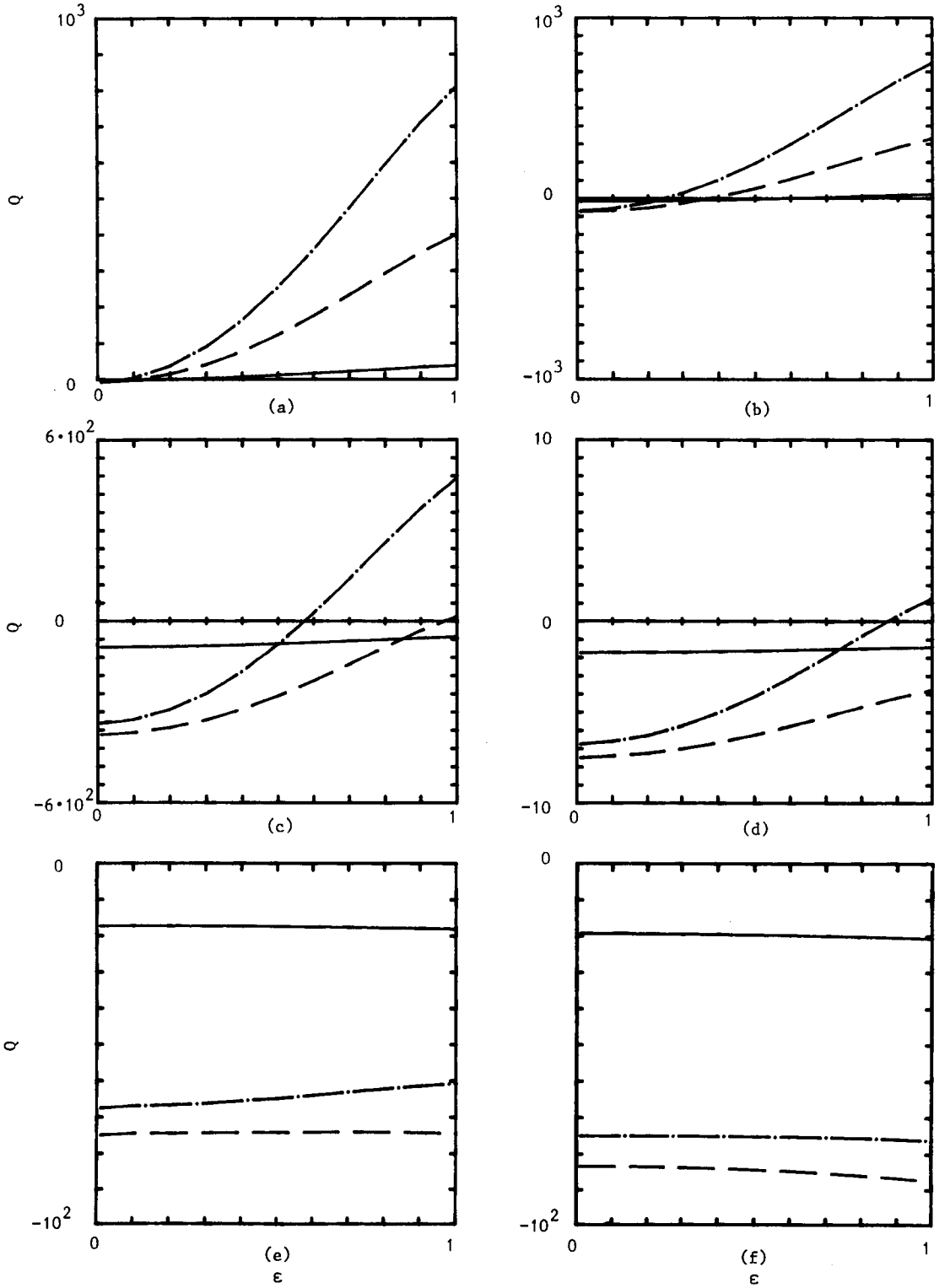

Figure 13. Vertical heat flux vs scaled temperature difference between the boundaries. —— $\alpha = 0.01$, – – – $\alpha = 0.1$, —·— $\alpha = 0.2$. (a) $\Gamma = 2 \times 10^{-4}$, (b) $\Gamma = 2 \times 10^{-3}$, (c) $\Gamma = 10^{-2}$, (d) $\Gamma = 2 \times 10^{-2}$, (e) $\Gamma = 0.2$, (f) $\Gamma = 2$.

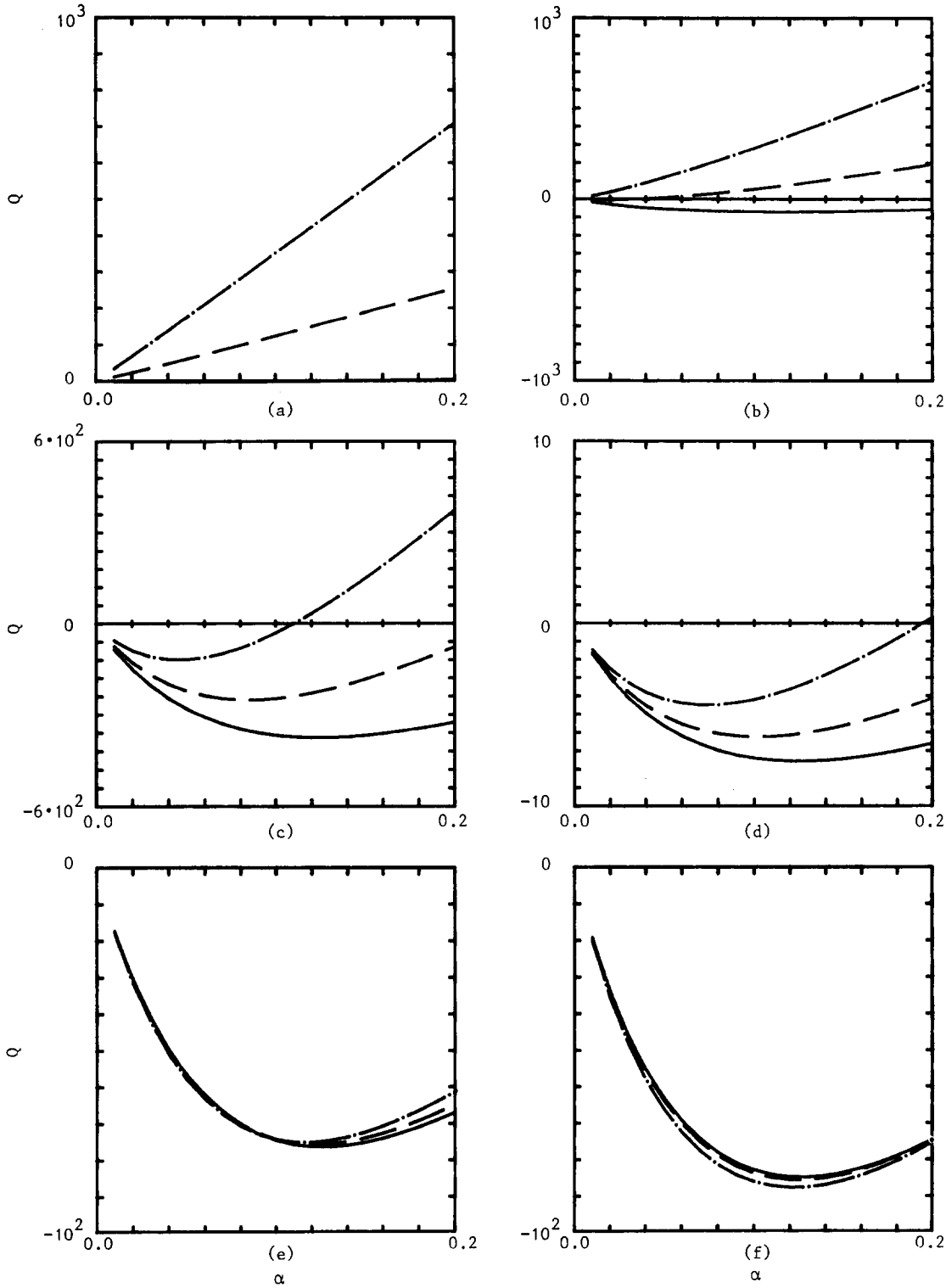

Figure 14. Vertical heat flux vs volume fraction of particles. —— $\epsilon = 0.1$, —— $\epsilon = 0.5$, —·— $\epsilon = 0.9$. (a) $\Gamma = 2 \times 10^{-4}$, (b) $\Gamma = 2 \times 10^{-3}$, (c) $\Gamma = 10^{-2}$, (d) $\Gamma = 2 \times 10^{-2}$, (e) $\Gamma = 0.2$, (f) $\Gamma = 2$.

This is possible due to the density variation of the gas over the cavity width, with a downward heavy gas flow in the cold wall region and an upward light gas flow in the hot wall region.

As is seen from figures 9–12, the mass flux of the gas is but a small fraction of the total mass flux for $\Gamma \geqslant 2 \times 10^{-3}$. The mass flux of the dispersed phase is thus essentially represented by the total mass flux, except for $\Gamma = 2 \times 10^{-4}$, and is therefore not presented here.

The total vertical heat flux of the two-phase flow as a function of ϵ and α for various Γ-values is shown in figures 13 and 14. As can be seen, it may be positive as well as negative (in the upward or downward direction), whereas it is always positive for single-phase flow in a closed slot (Chenoweth & Paolucci 1985). In the present case the direction and magnitude of the heat flux are primarily controlled by Γ and secondarily by ϵ and α.

At small values of Γ, e.g. 2×10^{-3} and 2×10^{-3}, the flow is controlled by the convection process in the mixture with insignificant relative velocities between the phases. The heat flux is mostly positive and increases with growing temperature difference ϵ and volume fraction α.

At intermediate values of Γ, e.g. 10^{-2} and 2×10^{-2}, both the effect of thermal convection and the gravitational separation are important. The heat flux may be in either direction, depending on the values of ϵ and α. It is still increasing with growing ϵ, but reaches a minimum at a certain value of α, depending on ϵ.

At large values of Γ, e.g. 0.2 and 2, the flow becomes dominated by the gravitational separation of the phases, which gives entirely negative and ϵ-independent heat fluxes. A minimum of the vertical heat flux (maximum magnitude) is reached at the value of $\alpha \sim 0.12$.

5. SOME GENERAL CONCLUSIONS

The main result of the present investigation is that the flow pattern in each phase as well as the overall vertical mass and heat fluxes in the mixture are essentially controlled by a dimensionless parameter Γ—the ratio of the relative velocity between the phases to the convection velocity in the gas. Specifically:

(1) At *small* values of Γ the effect of thermal convection is dominating which results in a countercurrent flow of each phase with a nearly antisymmetric velocity distribution, which for the small temperature differences reduces to the well-known cubic velocity profile of Batchelor (1954). It is noteworthy that the heat and mass transfer in the mixture are in *different* directions in this case. The total mass flux is negative (directed downwards) and reaches a minimum (maximum magnitude) when the volume concentration of particles $\alpha \sim 0.12$. The vertical heat flux of the mixture is positive (directed upwards).

(2) At *intermediate* values of Γ, both the effect of thermal convection and phase separation are of importance. This gives various types of velocity profiles, distinct for each phase and increasingly asymmetric with growing Γ-values. The total mass flux is negative and becomes temperature independent. A minimum (maximum magnitude) of the mass flux is reached at $\alpha \sim 0.12$. The vertical heat flux is mostly negative (directed downwards) and increases with growing temperature difference ϵ between the walls. A minimum of the heat flux is obtained for various values of α depending on ϵ.

(3) When the values of Γ are *large* the mixture flow is dominated by the effect of phase separation. We thus obtain an upward flow gas with an almost parabolic velocity profile and a downward flow of particles with a strongly asymmetric, due to the viscosity variation, velocity distribution over the slot width. Mass and heat fluxes become entirely negative and insensitive to the temperature difference variations. Extreme values (negative minima) of the mass and heat fluxes are again reached at $\alpha = 0.12$.

REFERENCES

BATCHELOR, G. K. 1954 Heat transfer by free convection across a closed cavity between vertical boundaries at different temperatures. *Q. appl. Math.* **12,** 209–233.

CHENOWETH, D. R. & PAOLUCCI, S. 1985 Gas flow in vertical slots with large horizontal temperature differences. *Phys. Fluids* **28,** 2365–2374.

DI GIOVANNI, P. R. & LEE, S. L. 1974 Impulsive motion in a particle–fluid suspension including particulate volume, density and migration effects. *J. appl. Mech.* **41,** 35–41.

DREW, D. A. 1971 Averaged field equations for two-phase media. *Stud. appl. Math.* **L,** 133–166.
DREW, D. A. 1983 Mathematical modeling of two-phase flow. *A. Rev. Fluid Mech.* **15,** 261–291.
DREW, D. A. & LAHEY, R. T. 1979 Application of general constitutive principles to the derivation of multidimensional two-phase flow equations. *Int. J. Multiphase Flow* **5,** 143–264.
ISHII, M. 1975 *Thermo-fluid Dynamic Theory of Two-phase Flow*, Eyrolles, Paris.
KYNCH, G. J. 1952 A theory of sedimentation. *Trans. Faraday Soc.* **48,** 166–176.
NIGMATULIN, R. I. 1979 Spatial averaging in the mechanics of heterogeneous and dispersed systems. *Int. J. Multiphase Flow* **5,** 353–385.
RUBINOW, S. I. & KELLER, J. B. 1961 The transverse force on a spinning sphere moving in a viscous fluid. *J. Fluid Mech.* **11,** 447–459.
SAFFMAN, P. G. 1965 The lift on a small sphere in a slow shear-flow. *J. Fluid Mech.* **22,** 385–400.
TAM, K. W. 1969 The drag on a cloud of spherical particles in low Reynolds number flow. *J. Fluid Mech.* **38,** 537–546.
WALLIS, G. B. 1969 *One-dimensional Two-phase Flow*. McGraw-Hill, New York.
WHITE, F.M. 1974 *Viscous Fluid Flow*. McGraw-Hill, New York.
ZUBER, N. 1964 On the dispersed two-phase flow in a laminar flow region. *Chem. Engng Sci.* **19,** 897–917.

APPENDIX A

Constant Conductivity and Viscosity Case

Solution of the energy equation [36] gives in this case a well-known linear temperature distribution between the boundaries:

$$\theta = 1 + \epsilon(2\xi - 1). \qquad [A.1]$$

Introducing [A.1] into [35] and integrating twice we express the velocity of the continuous phase as a function of the transverse coordinate ξ,

$$V_c(\xi) = \lambda\Gamma^{-1}\{\epsilon^{-2}/4\,(1-\epsilon+2\epsilon\xi)\,[\ln(1-\epsilon+2\epsilon\xi)-1] - [1+\gamma(P-\alpha)/(1-\alpha)]\xi^2/2 + c_1\xi + c_2\}. \qquad [A.2]$$

Constants c_1 and c_2 are then obtained by means of the boundary conditions

$$V_c(0) = V_c(1) = 0,$$

giving

$$c_1 = [1+\gamma(P-\alpha)/(1-\alpha)]/2 + \epsilon^{-2}\{(1+\epsilon)[1-\ln(1+\epsilon)] + (1-\epsilon)[\ln(1-\epsilon)-1]\}/4 \qquad [A.3]$$

and

$$c_2 = \epsilon^{-2}(1-\epsilon)[1-\ln(1-\epsilon)]/4. \qquad [A.4]$$

Finally, the pressure term P is given by the zero total flux condition [34],

$$P = \{\epsilon^{-3}(1+\epsilon)^2[1/2-\ln(1+\epsilon)]/16 + \epsilon^{-3}(1-\epsilon)^2[\ln(1-\epsilon)-1/2]/16 + \epsilon^{-2}/4 - [1-\gamma\alpha/(1-\alpha)]/12 - \epsilon^{-2}(1+\epsilon)[1-\ln(1+\epsilon)]/8 + \epsilon^{-2}(1-\epsilon)[1-\ln(1-\epsilon)]/8 + \Gamma\alpha^2/(\lambda f)\}/\{\gamma/[12(1-\alpha)] + \Gamma\alpha^2/(\lambda f)\}. \qquad [A.5]$$

APPENDIX B

Variable Conductivity and Viscosity Case

In this case we assume that the nondimensional conductivity k^* and viscosity μ^* are functions of the temperature θ according to [37] and [38]. The temperature distribution is then obtained by means of [36] and [37] and is no longer linear:

$$\xi = (1+S_k)/c_1\,[2S_k^{3/2}\arctan(\theta/S_k)^{1/2} + 2S_k^{1/2}(\theta/3 - S_k)] - c_2/c_1, \qquad [B.1]$$

where

$$c_1 = (1 + S_k)[2S_k^{3/2} \arctan(\theta_1/S_k)^{1/2} + 2\theta_1^{1/2}\ (\theta_1/3 - S_k)] - c_2 \qquad [B.2]$$

and

$$c_2 = (1 + S_k)[2S_k^{3/2} \arctan(\theta_0/S_k)^{1/2} + 2\theta_0^{1/2}(\theta_0/3 - S_k)]. \qquad [B.3]$$

The form of [B.1] suggests the use of θ as an independent variable. Introducing [37] and [38] into [35] and integrating with respect to θ we obtain the velocity of the continuous phase as function of temperature:

$$V_c(\theta) = \lambda\Gamma^{-1}(1 + S_k)^2 c_1^{-2}/(1 + S_\mu)[\{2 + 2S_k[1 + \gamma(P - \alpha)/(1 - \alpha)]\} \times [f_1(\theta) - S_k^{1/2} f_2(\theta)] - 2/3[1 + \gamma(P - \alpha)/(1 - \alpha)] f_3(\theta) + c_3 f_4(\theta) + c_4], \qquad [B.4]$$

where

$$f_1(\theta) = 2/3\ \theta^{3/2} + 2(S_\mu - S_k)\theta^{1/2} - 2(S_\mu - S_k)S_k^{1/2} \arctan(\theta/S_k)^{1/2}, \qquad [B.5]$$

$$f_2(\theta) = (\theta + S_k)\arctan(\theta/S_k)^{1/2} - (S_k\theta)^{1/2} + 2(S_\mu - S_k)\int z \tan z\ dz, \qquad [B.6]$$

where $z = \arctan(\theta/S_k)^{1/2}$

$$f_3(\theta) = 2/5\ \theta^{5/2} + 2S_k^{3/2}(S_\mu - S_k)\arctan(\theta/S_k)^{1/2} + 2(S_\mu - S_k)\theta^{1/2}(\theta/3 - S_k), \qquad [B.7]$$

$$f_4(\theta) = \theta + (S_\mu - S_k)\ln(S_k + \theta), \qquad [B.8]$$

$$c_3 = -\{2 + 2S_k[1 + \gamma(P - \alpha)/(1 - \alpha)]\}a_1 + 2/3[1 + \gamma(P - \alpha)/(1 - \alpha)]a_2, \qquad [B.9]$$

$$c_4 = \{2 + 2S_k[1 + \gamma(P - \alpha)/(1 - \alpha)]\}[-f_1(\theta_0) + a_1 f_4(\theta_0)] + 2/3[1 + \gamma(P - \alpha)/(1 - \alpha)][f_3(\theta_0) - a_2 f_4(\theta_0)], \qquad [B.10]$$

$$a_1 = [f_1(\theta_1) - f_1(\theta_0)]/[f_4(\theta_1) - f_4(\theta_0)] \qquad [B.11]$$

and

$$a_2 = [f_3(\theta_1) - f_3(\theta_0)]/[f_4(\theta_1) - f_4(\theta_0)]. \qquad [B.12]$$

It is now possible to obtain an expression for the pressure term by means of [34]:

$$P = (1 - \alpha)\{[(1 + S_k)/\gamma - S_k\alpha/(1 - \alpha)][-I_1 + a_1 I_4 + f_1(\theta_0)I_5 - a_1 f_4(\theta_0)I_5] + 1/3[1/\gamma - \alpha/(1 - \alpha)][I_3 - a_2 I_4 - f_3(\theta_0)I_5 + a_2 f_4(\theta_0)I_5] + 1/2(\alpha\delta c_1)^2(1 + S_k)^{-2}/(f\lambda)I_6\}/\{S_k I_1 - S_k a_1 I_4 - S_k f_1(\theta_0)I_5 + S_k a_1 f_4(\theta_0)I_5 - I_3/3 + a_2 I_4/3 + f_3(\theta_0)I_5/3 - a_2 f_4(\theta_0)I_5/3 + (1 - \alpha)(\alpha\delta c_1)^2(1 + S_k)^{-2}/(f\lambda)I_6\}, \qquad [B.13]$$

where

$$I_j = \int_{\theta_0}^{\theta_1} f_j(\theta)\, d\theta, \qquad j = 1, \ldots, 4, \qquad [B.14]$$

$$I_5 = 2S_k^{3/2}[\arctan(\theta_1/S_k)^{1/2} - \arctan(\theta_0/S_k)^{1/2}] + 2\theta_1^{1/2}(\theta_1/3 - S_k) - 2\theta_0^{1/2}(\theta_0/3 - S_k) \qquad [B.15]$$

and

$$I_6 = f_4(\theta_1) - f_4(\theta_0). \qquad [B.16]$$